

## Modular Multilevel Photovoltaic Interfaced Converter with Low Voltage Energy Integration for DC Systems

Gagić, Mladen; Huang, Kewei; Qin, Zian; Ferreira, Bram

**DOI**

[10.1109/ICDCM45535.2019.9232895](https://doi.org/10.1109/ICDCM45535.2019.9232895)

**Publication date**

2019

**Document Version**

Final published version

**Published in**

2019 IEEE Third International Conference on DC Microgrids (ICDCM)

**Citation (APA)**

Gagić, M., Huang, K., Qin, Z., & Ferreira, B. (2019). Modular Multilevel Photovoltaic Interfaced Converter with Low Voltage Energy Integration for DC Systems. In *2019 IEEE Third International Conference on DC Microgrids (ICDCM): Proceedings* Article 9232895 IEEE.  
<https://doi.org/10.1109/ICDCM45535.2019.9232895>

**Important note**

To cite this publication, please use the final published version (if applicable).  
Please check the document version above.

**Copyright**

Other than for strictly personal use, it is not permitted to download, forward or distribute the text or part of it, without the consent of the author(s) and/or copyright holder(s), unless the work is under an open content license such as Creative Commons.

**Takedown policy**

Please contact us and provide details if you believe this document breaches copyrights.  
We will remove access to the work immediately and investigate your claim.

# Modular Multilevel Photovoltaic Interfaced Converter with Low Voltage Energy Integration for DC Systems

Mladen Gagic, Kewei Huang, Zian Qin, Braham Ferreira  
Electrical Sustainable Energy  
Delft University Of Technology  
Delft, the Netherlands  
m.gagic@tudelft.nl

**Abstract**—This paper presents a multilevel, cascaded converter topology that allows for integrations of combined photovoltaic and battery storage units. The modular features of the system enable the series connection of PV panels that, in turn, have a parallel connection to a specified voltage level. These voltage levels stem from a series string of power electronic submodules. Likewise, low voltage energy storage units are interfaced to the upper arm of the system via identical converter modules and provide various directions of dc and ac active power flow, depending on the mode of operation. By implementing additional, nested current loops, guided by passive filters, the system controls the power flow between the photo-voltaic string, batteries and the low voltage dc terminal. The enhanced level of power flow allows the converter to achieve both a controlled energy exchange as well as various auxiliary services in the DC system. This paper demonstrates three distinct types of power flow that are achievable with by combining the multilevel topology along with multifrequency operations. Simulation results from a representative system model are utilised to demonstrate the three possible modes of operation.

**Keywords**—LV dc, photo-voltaic, energy-storage, cascade, modularity, multifrequency, power flow control.

## I. INTRODUCTION

With the gradual proliferation of dc systems [1]–[3], novel methods of power delivery are a key requirement for distributed, renewable energy sources that have inherent dc properties. Likewise, the incorporation of energy storage units is crucial for any dc microgrid (MG) that consists of stochastic sources of electrical energy. The conventional method of ascertaining such a system would include having separate converters for interfacing the various elements such as photovoltaic (PV) and battery electrical storage (BES) [4]–[7]. Within such a system, one of the difficulties relates to the fact that each type of device requires a separate converter which is most often optimised for the voltage and power level of the dc system and the interfacing device in question. Although this approach is convenient when picking and installing readily available power electronics (PEs) converters with standardised operational parameters, various issues related to system control and compatibility can become a greater issue with an increase in the variability of converter types and ratings within the system. These issues stem from the fact that the interaction between the converters has a proclivity to cause unwanted circulating currents, instability in certain operating conditions and general difficulty related to communication and control protocols. Likewise, with a multi-voltage system, as are usually the case in more complex designs, the greater variety of voltage and power levels entails more converter types that need to be employed. This, in turn, increases the complexity of monitoring and maintenance of the system.

One method of addressing this issue is the incorporation of both PV sources and BES elements within a single topology, with minimum additional conversion stages. Among the solutions currently present are devices that implement either a single PE converter that simultaneously interfaces both elements to the grid [8]–[9] or a converter that balances the power flow within its dc link with the dc system. Although these topologies provide a remedy for the compatibility and integration issue mentioned previously, various compromises to the system properties are required in order to accommodate both the PV and BES systems. First and foremost are the limitations that relate to the expandability and/or upgradability of such a system. Since the power and voltage levels of these devices are essentially limited to predetermined values, any modification to the PV unit or BES system would be required to remain within a predetermined range. Likewise, in case of a fault on the converter, both of the devices could be put offline.

Recently, these issues have been mitigated by implementing a modular/cascaded approach to converter design. Systems that interface BES to identical converter submodules (SMs) have been presented in [10]–[16], while similar systems that incorporate PV modules to SMs have also been explored in [17]–[22]. Such systems are expandable via the addition of extra modulus in either series or parallel, in order to maintain or alter the voltage/current rating of the design. Although these systems have various benefits when interfacing either exclusively PV or BES, the combination of these two devices requires that an additional converter be introduced in the system in order to interface the respective complimentary device. This entails that the system still requires an additional converter that must be rated to either the full voltage or full current rating of the system. Therefore, the modularity of these systems essentially extends to only one dimension and as a consequence, these topologies generally lack a cohesive expandability in terms of both PV and BES.

With these limitations in mind, the newly introduced Modular Multilevel DC Converter [23]–[25] is a topology that allows for power conversion on multiple levels. This is possible via a secondary (nested) current loop, within the topology that is guided by passive or active tuned filters. As a result, the converter has the potential to incorporate a greater number of dc terminals in a certain design. More crucially, various dc devices such as sources, loads and storage elements can interface to either the main dc terminal or, the submodules that comprise the string. Based on this principle, the incorporation of series-connected PV panels and battery interfacing submodules is explored in this paper.

The layout of this paper is as followed: Section II briefly describes the topology and the key principles of operation

related to the M2DC. In section III, three different modes of operation of this converter are presented and discussed. The fourth and fifth section provides the simulation results of a model system and conclusions respectively.

## II. PRINCIPLE OF OPERATION

The Modular Multilevel DC Converter [23]–[25] (M2DC) represents a power electronics converter that emerged from the concept of implementing additional (nested) current loops [23] within a conventional modular multilevel design. These additional current loops act as a substitute for the low frequency (50/60 Hz) component that would otherwise be present in conventional MMC systems. By implementing this secondary ac current loop, the converter achieves charge balancing of the submodule capacitors, along with other benefits that will be discussed in this paper.

A basic topology of a single leg M2DC is presented in Fig.1. As is visible from the layout the converter consists of two dc terminals, one of which is a lower-voltage (LV) and the second a higher-voltage (HV) connection. In the case of this topology, passive filters guide the circulating ac current. The first is a band-pass filter located across the string of SMs, and the other a band-stop filter situated between the LV terminal and the cross-section of the two converter arms. Additionally, an arm inductance is situated in between the upper and lower arm of the converter. This inductance is relevant to the converter operation, as will be discussed in this section.

The converter operates by controlling the injected ac and dc voltage of the upper and lower arm submodules. Therefore, the power transfers between the terminals and submodules via a combination of dc and ac current components, making this a multifrequency network [24], [26]. The control system regulates the upper and lower converter arms separately by multiplying the injected voltage references (1) and (2) with the sum of the respective capacitor voltages ( $V_{cu}$  and  $V_{cl}$ ). For a two-arm system (upper and lower), such as the one explored in this paper, parameters  $D_u$  and  $D_l$  denote the inserted dc component reference of the upper and lower converter arm respectively. Likewise,  $m_u$  and  $m_l$  represent the inserted ac component reference of the two arms required to generate the secondary circulating current. This current has an angular frequency of  $\omega$  and is also defined by the phase difference  $\varphi$  between the upper and lower arm. These parameters provide the combined ac and dc upper and lower arm injected

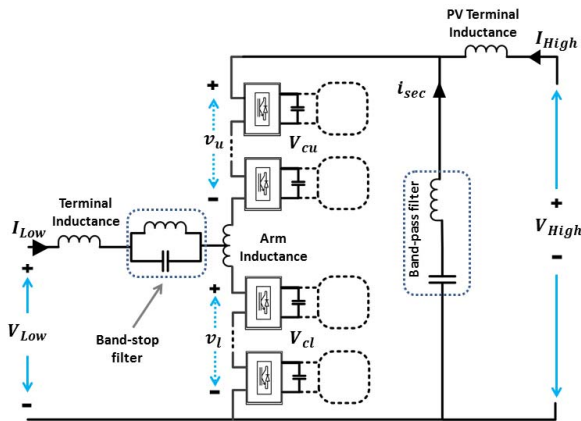


Fig. 1. Single-arm Modular Multilevel DC Converter

voltage, given by (3) and (4).

$$u_{ref\_u} = D_u - m_u \cdot \cos(\omega t + \varphi) \quad (1)$$

$$u_{ref\_l} = D_l + m_l \cdot \cos(\omega t) \quad (2)$$

$$v_u = V_{cu} \cdot D_u - V_{cu} \cdot m_u \cdot \cos(\omega t + \varphi) \quad (3)$$

$$v_l = V_{cl} \cdot D_l + V_{cl} \cdot m_l \cdot \cos(\omega t) \quad (4)$$

These equations are expandable for systems that consist of multiple arms. The following section addresses how the control of parameters ( $D_u$ ,  $D_l$ ,  $m_u$ ,  $m_l$  and  $\cos(\varphi)$ ) achieves the various control goals of this system. The secondary current for this specific topology, where the converter arms are predominantly inductive is given by (5). This inductive quality allows the converter to operate in unison with the PV string as a voltage control current source. The converter is by default bidirectional, enabling the delivery of power from either of the two terminals. More crucially, the individual converter submodules have the potential to interface and exchange power with various types of devices such as load, sources or storage units.

$$i_{sec} = \frac{[V_{cu} \cdot m_u \cdot \sin(\omega t + \varphi) - V_{cl} \cdot m_l \cdot \sin(\omega t)]}{\omega L_{arm}} \quad (5)$$

## III. RANGE OF OPERATION

For the purpose of mitigating the issues related to interfacing various devices to a dc microgrid, as described in Section I, the initial design of the M2DC Fig.1 is configured to accommodate PV cells and BES units. As a result, a multilevel converter that incorporates these two types of devices is configured and presented in Fig.2. This configuration of the M2DC consists of series-connected PV cells across the higher voltage terminal. Likewise, the systems incorporate energy storage devices such as batteries, by interfacing them to submodules across the upper converter arm. Finally, the low voltage terminal is considered to be connected to a constant dc voltage, which represents a low or medium voltage microgrid. The remainder of the converter system is unaltered, with the band pass and band stop filters location unchanged.

For this design, the submodules of the lower arm implement a half-bridge configuration as in Fig.3. Due to this, the dc component of the injected voltage should always be equal to or greater than the ac component. The application of a half-bridge configuration for the submodules reduces the complexity of the topology and lowers the semiconductor losses associated with switching. Since the lower converter arm SMs are not interfacing any device, they mirror the terminal voltage of the converter with (6).

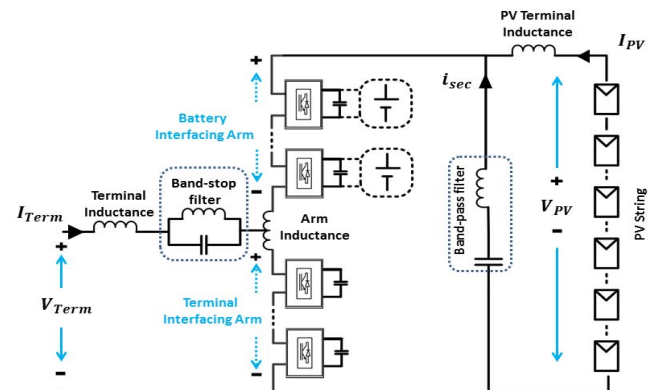


Fig. 2. Photovoltaic interfaced Modular Multilevel DC Converter with integrated low voltage battery energy storage

$$V_{term} = V_{cl} \cdot D_l \quad (6)$$

Unlike the lower arm submodules, the upper arm converter SMs are chosen as a full-bridge topology. This greatly increases the range of voltage the converter can provide. Likewise, the available level of power flow between the interfacing BES and the remaining converter is also increased. By implementing a full-bridge configuration, additional fault and protection features can also be become available.

In this type of design, the system incorporates both PV sources as well as BES with at least one dc terminal within a single configuration. The controller of this system must cover several levels of control. At the top level, the controller deals with the maximum power-point tracking requirement of the system and therefore should take president. By contrast, the second level of control is dependent on the specific mode in which the converter is operating. These modes are among others:

- Direct power delivery from the PV sources onto the grid, with a net zero power exchange with the batteries.
- Inter-power exchange between the PV sources and BES along with power delivery to the dc grid.
- Charging of the BES via the PV sources and dc grid power.

#### A. Primary Control Level: Maximum Power Point Tracking

In order to achieve MPPT tracking, the voltage across the PV string needs to be modified within a certain range. The high output voltage of the terminal interfacing the string of PV submodules is determined by the sum of the injected arm dc voltage (7).

$$V_{PV} = D_l \cdot V_{cl} + D_u \cdot V_{cu} \quad (7)$$

Since the low voltage terminal is considered to be a fixed dc grid, the dc voltage injection of the lower arm is constant and equal to  $V_{term}$ . Therefore, any voltage change across the higher-voltage terminal is determined by the injected dc voltage component of the upper arm ( $V_{cu} \cdot D_u$ ). The sum of the upper arm submodule dc capacitor voltages is determined by the voltage levels of the energy sources that the submodule interfaces. This voltage range is dependent on the LV dc terminal as well as the chosen voltage value and number of BES submodules. If the BES are chosen such that their sum is equal or greater than the LV dc terminal, the positive voltage levels that can be achieved across the string of PV panels range from zero to the full voltage ( $V_{term} + \sum V_{BES}$ ) for ( $D_u \rightarrow 1$ ). Likewise, the lowest voltage at the higher-terminal is then equal to zero or a negative value. This enables the system to operate in the wide range required for the MPPT of the PV panels.

Therefore, in order to adjust the voltage across the string of PV cells, the system must modify the injected voltage of the upper arm by means of the relevant dc arm reference. Since the ac injection reference range of the upper converter arm ( $m_u$ ) is determined by this value, the second level control is subject to any parameter change that occurs on the primary (MPPT) level.

#### B. Secondary Level of Control: Power Flow Control

There are three distinct sources of power in the presented system, the BES units, the low voltage dc terminal and the

string of PV sources. While the first two can be considered bidirectional, the PV source can only inject power equal to or greater than zero. The M2DC system allows for several degrees of power flow, that can be modified and adjusted via multiple parameters, with several having a direct or indirect effect of the others.

By multiplying the upper arm current, consisting of the PV output current and secondary (circulating) current with the injected arm voltage of the converter, the average active power can be calculated. This is achieved by averaging over a period of the secondary frequency. As a result, the active power balance of the upper arm string of submodules is equal to (8).

$$P_u = V_{cu} \cdot D_u \cdot I_{PV} - \frac{V_{cu} \cdot m_u \cdot V_{cl} \cdot m_l \cdot \sin(\varphi)}{2\omega \cdot L_{arm}} \quad (8)$$

Since the upper converter arm submodules can inject positive and negative voltage, the BES can sink or source the dc power component ( $V_{cu} \cdot D_u \cdot I_{PV}$ ). Likewise, the ac active power component of (8) can be either positive or negative, depending on the value of  $m_u$  and  $\varphi$ . This enables the system to have a greater degree of power flow with respect to the charging and discharging of batteries.

Apart from these main control goals, the operation of the system should ensure a high level of efficiency. One key method of achieving this is by setting the circulating current (required for the power transfer) as low as possible while still being subject to the primary and secondary level of control. For this reason, the ac voltage injection references ( $m_u, m_l$ ) should be set as high as possible, so that the circulating current is reduced for the same active power transfer.

Depending on the relationship between the three powers, the system can operate in three modes of operation:

- Direct power delivery.
- Inter-power exchange.
- Combined battery charging.

The direct power delivery mode is such that all the power being generated by the string of PV panels is transmitted to the dc terminal. Therefore, the power exchange with the BES is equal to zero. To achieve this mode of operation, after the primary level had set the values of  $D_l$  (required for the MPPT operation), the secondary control level needs to assure that (8) is equal to zero. Since the dc power component is determined by the PV current and the subsequent dc voltage injection (all dictated by the primary level of control), the second component of (8) is utilized to ensure zero active power exchange with the BES. Parameters  $V_{cu}$  and  $V_{cl}$  are determined by the voltage levels of the batteries and the dc terminal respectively, while  $m_u$  and  $m_l$  are intended to be kept as high as possible. This implies that the main parameter with which the power balance of the BES interfacing SM should be achieved is the phase-angle  $\varphi$ .

If the system tracks the PV current from the string of submodules and assumes or measures the voltage at the output dc terminals as well as the BES capacitor voltage, the secondary controller acts so that it sets the phase-angle, such that the conditions of (8) are met. When these conditions are met, the power that is generated by the PV string is equal to the output power on the dc terminal, in addition to some

losses in the process. Although the BES interfacing SMs are processing power, the net exchange is equal to zero.

In the inter-power exchange mode, power from the string of PV modules and the BES is combined and a certain amount is derived to the dc terminal. This implies that the net power balance between the BES and the system is not zero, meaning that (8) should be equal to the amount of power that the BES is delivering to the dc terminal or extracting from the PV power. Similar to the previous mode of operation, the PV current and the injected dc voltage are determined by the primary control level. Therefore, by setting the active power of the ac component, the total active power exchange between the BES and the system is determined. As in the previous case, the phase angle should be implemented primarily to set this power exchange to a level determined by the system or controller.

Lastly, since the system is designed to be bidirectional, the power from the dc terminal can be reversed and in combination with the PV power, utilised to charge the BES in the upper arm of the converter. To achieve this, the phase angle of the second active power component of (8) should be greater than the dc power component. Under these conditions, the current from the dc terminal changes signs and contributes to the power delivery to the BES units.

#### IV. SIMULATION RESULTS

To demonstrate the combined power exchange between a photovoltaic source, low voltage dc grid and battery storage units, this paper utilizes a model system designed in *Simulink*. The system, presented in Fig. 3, consists of a four-submodule M2DC converter, with full-bridge submodules placed in the upper arm and two half-bridge submodules in the lower converter arm. The upper arm SMs are each interfaced to constant dc voltage sources that represent a 48V battery, while the lower SMs remain open such as in conventional MMCs. In this model, it is taken that the converter is interfacing a stiff, low voltage dc grid on the low-voltage terminal. Three photovoltaic sources are connected in series across the high-terminal of the converter. These sources are taken from pre-existing libraries that simulate the behaviour of photovoltaic cells. The solar power to each cell is constant and chosen to be maximum for these experimentations. All relevant simulation parameters are provided in Table I.

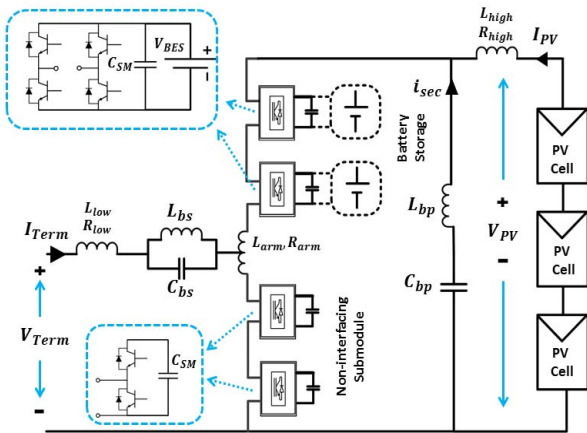


Fig. 3. Simulation setup of photovoltaic interfaced Modular Multilevel DC Converter with integrated battery energy storage.

#### A. Photovoltaic Power Delivery During Voltage Sweep

As was stated in the previous section, the MPPT tracking is achieved by varying the voltage across the string of submodules. The main parameter for altering the PV voltage is the dc injection reference for the upper converter arm ( $D_u$ ). By changing this voltage reference at a rate given by Fig. 4, the sum voltage across the PV string varies from 0V to 88.8V, as seen in Fig. 5.a The resulting current from the PV string is given in Fig. 5.b and drops-off increasingly fast after a certain point, which is expected from a PV system. The converter secondary current, at Fig. 5.c is the result of the ac active power exchange between the upper converter arm and the lower arm. Since the remaining parameters of the converter remain constant during the sweep, the secondary current remains fairly constant during the process. As a result of the change in voltage across the PV string, the photovoltaic power curve is given in Fig. 6. Therefore, by modifying  $D_u$ , MPPT can be achieved within the converter. The terminal current given in Fig. 7 is positive, implying that the grid is delivering power to the converter and storing it into the BES. This represents the third mode of the converter, discussed in the previous section.

TABLE I. PARAMETERS AND VALUES OF SIMULATED SYSTEM

Symbols	Descriptions	Value
$V_{PV}$	Photovoltaic string voltage	Variable
$I_{PV}$	Photovoltaic string current	Variable
$I_{Term}$	Grid-terminal current	Variable
$i_{sec}$	Secondary current/ circulating current of the secondary power loop	Variable
$V_{Term}$	Grid-terminal voltage	48 V
$V_{BES}$	Nominal battery voltage source	48 V
$V_{OC}$	Photovoltaic open circuit voltage	28 V
$V_{MP}$	PV voltage at maximum power point	26 V
$I_{SC}$	Photovoltaic short circuit current	1 A
$I_{MP}$	PV current at maximum power point	0.85 A
$C_{SM}$	Submodule capacitance	200 $\mu C$
$L_{bp}$	Band-pass filter inductance	98 $\mu H$
$C_{bp}$	Band-pass filter capacitance	67.7 $\mu C$
$L_{bs}$	Band-stop filter inductance	1464 $\mu H$
$C_{bs}$	Band-stop filter capacitance	4.55 $\mu C$
$R_{arm}$	Equivalent upper arm resistance (sum of upper arm inductor resistance and switch turn on resistance)	135 m $\Omega$
$L_{arm}$	Arm inductance	990 $\mu H$
$R_{PV}$	PV terminal equivalent resistance	333 m $\Omega$
$L_{PV}$	PV terminal equivalent inductance	2894 $\mu H$
$R_{Term}$	Grid terminal equivalent resistance	134 m $\Omega$
$L_{Term}$	Grid terminal equivalent inductance	984.9 $\mu H$
$f_{sec}$	Secondary frequency	1.953 KHz
$f_{sw}$	Converter switching frequency	25 KHz

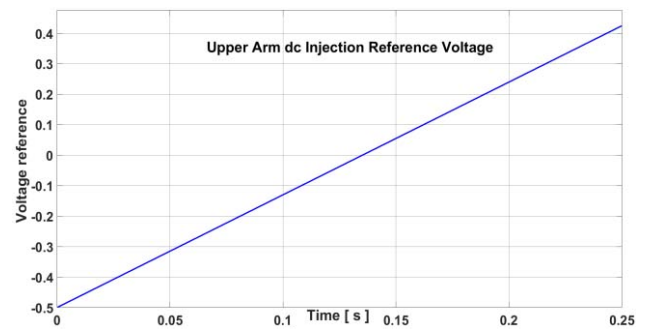


Fig. 4. Upper arm dc injection reference voltage sweep trajectory.

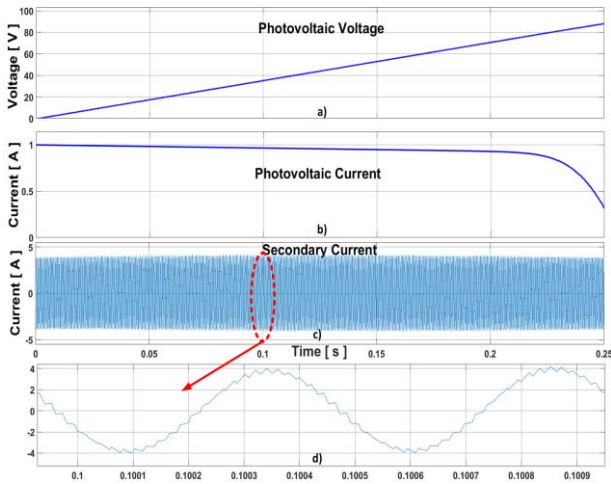


Fig. 5. Simulation results for upper arm voltage sweep  
 $m_u = m_l = D_l = 0.5$ ;  $\varphi = -1$  rad;  
 a) Photovoltaic voltage; b) Photovoltaic current;  
 c) Secondary/circulating current;  
 d) Zoomed-in secondary current.

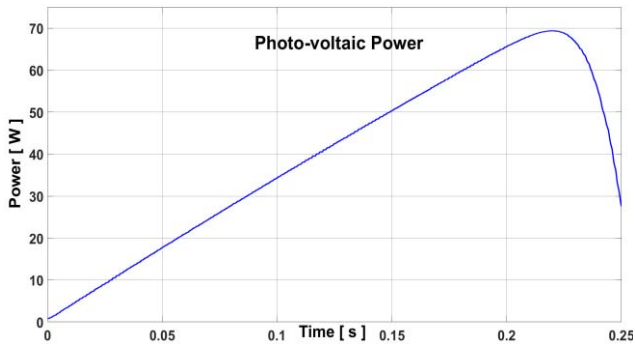


Fig. 6. Simulated photovoltaic power during upper arm voltage sweep.

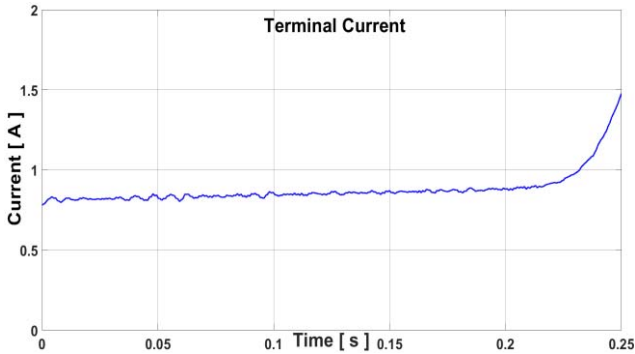


Fig. 7. Simulated terminal current for upper arm voltage sweep.

### B. Varying Power Delivery from BES Components

When the primary control level sets the parameters required for MPPT, the converter may adjust or set the secondary level of control to a certain type of power exchange. As previously stated, three parameters can be utilized for this purpose ( $m_u$ ,  $m_l$  and  $\varphi$ ). To demonstrate the different types of power flow capabilities within the converter, the  $D_u$  is set to provide the maximum power delivery from the PV string while the phase angle  $\theta$  ( $\varphi$ ) is varied from 1.57 rad to -1.57 rad as in Fig. 8.

As is visible in Fig. 9a,b the photovoltaic current and voltage remain relatively constant during this experiment, as does the power from the PV string given in Fig. 10. The

secondary current of the converter changes in amplitude as the BES alters the direction and quantity of power being delivered, as seen in Fig. 9.c. Initially, the energy storage units in the upper converter arm are delivering active power alongside the PV string to the low voltage dc grid terminal. As can be seen when the current from Fig. 11. is multiplied by the terminal voltage (48V), the initial power the M2DC converter delivers to the grid is approximately 96W. This implies that the BES is providing the 25W difference from the PV source, after accounting for the losses in the converter. At the point where the terminal current equals zero, all the power from the PV sources is delivered directly to the BES units (direct power delivery). From this point, further decreases in the upper arm phase-angle will dictate the amount of power the BES units receive from the dc grid. The maximum grid terminal active power in this example is approximately 24W, including the 69W from the PV system from Fig. 10. This final mode of operation represents previously mentioned combined battery charging mode.

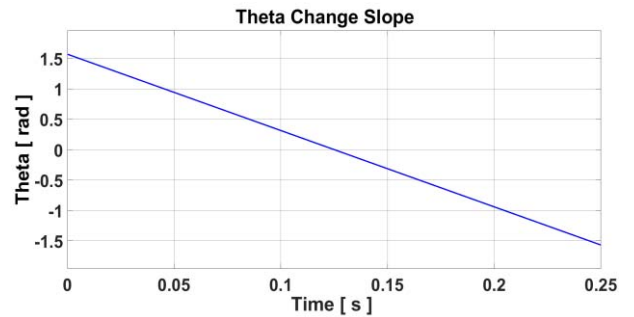


Fig. 8. Upper arm phase-angle ( $\varphi$ ) reference change during simulation.

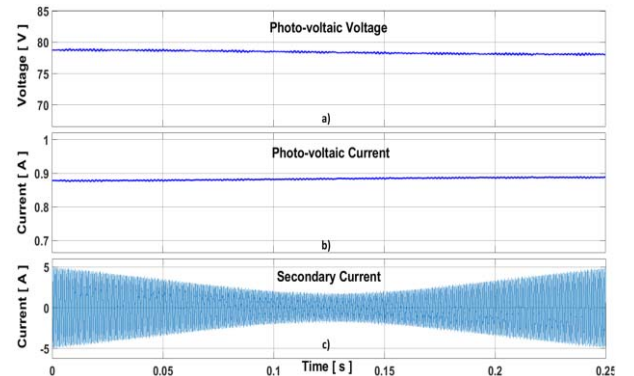


Fig. 9. Simulation results for upper arm phase angle sweep  
 $m_u = D_u = 0.375$ ;  $m_l = D_l = 0.5$   
 a) Photovoltaic voltage; b) Photovoltaic current;  
 c) Secondary/circulating current.

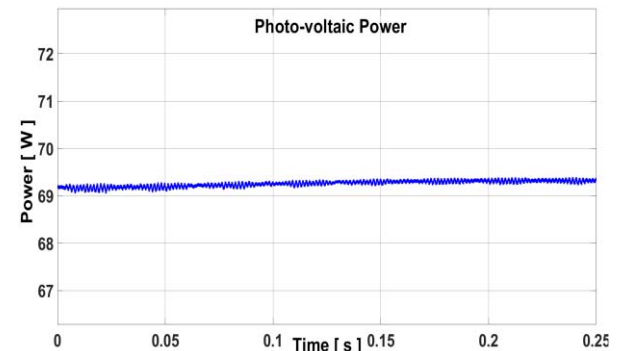


Fig. 10. Simulated photovoltaic power under upper arm phase-angle ( $\varphi$ ) sweep.

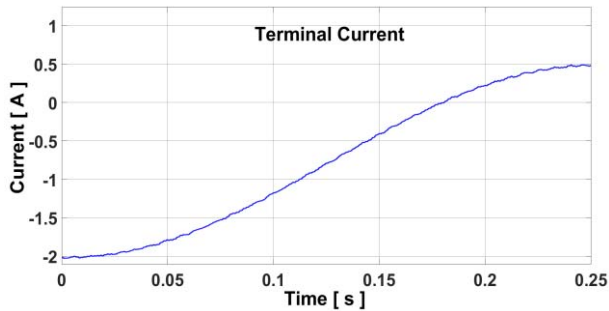


Fig. 11. Simulation of terminal current during upper arm phase-angle ( $\varphi$ ) sweep.

## V. CONCLUSION

The M2DC allows for the incorporation of both photovoltaic sources and energy storage units within a single, multilevel topology. Voltage adjustments required for MPPT can be done on one level of control by setting the upper arm dc voltage injection. By implementing circulating currents within the converter, the secondary control allows for various degrees of power flow between the different terminals and devices. Three modes of power flow are presented in this paper, including direct power delivery, inter-power exchange and combined battery charging. Simulation results demonstrating MPPT and all three modes of operation are provided in the paper.

## REFERENCES

- [1] L. Mackay, T. Hailu, L. Ramirez-elizondo, and P. Bauer, "Towards a DC Distribution System – Opportunities and Challenges," *2015 IEEE First Int. Conf. DC Microgrids*, pp. 215–220, 2015.
- [2] L. Mackay, T. G. Hailu, G. C. Mouli, L. Ram, J. A. Ferreira, and P. Bauer, "From DC Nano- and Microgrids Towards the Universal DC Distribution System – A Plea to Think Further Into the Future," 2015.
- [3] T. Hailu, L. Mackay, M. Gajic, and J. A. Ferreira, "From Voltage Stiff to Voltage Weak DC Distribution Grid: Opportunities and Challenges," *2016 IEEE 2nd Annu. South. Power Electron. Conf.*, pp. 1–6, 2016.
- [4] N. M. Nor, A. Ali, T. Ibrahim, and M. F. Romlie, "Battery Storage for the Utility-Scale Distributed Photovoltaic Generations," *IEEE Access*, vol. 6, pp. 1137–1154, 2017.
- [5] R. B. Bass, J. Carr, J. Aguilar, and K. Whitener, "Determining the Power and Energy Capacities of a Battery Energy Storage System to Accommodate High Photovoltaic Penetration on a Distribution Feeder," *IEEE Power Energy Technol. Syst. J.*, vol. 3, no. 3, pp. 119–127, 2016.
- [6] M. Takagi, Y. Iwafune, K. Yamaji, H. Yamamoto, K. Okano, R. Hiwatari, and T. Ikeya, "Economic value of PV energy storage using batteries of battery-switch stations," *IEEE Trans. Sustain. Energy*, vol. 4, no. 1, pp. 164–173, 2013.
- [7] W. Lawrance, "Shane Duryea, Syed Islam, and William Lawrance," *IEEE Ind. Appl. Mag.*, no. June, pp. 67–72, 2001.
- [8] S. J. Chiang, K. T. Chang, and C. Y. Yen, "Residential Photovoltaic Energy Storage System - Industrial Electronics, IEEE Transactions on," vol. 45, no. 3, pp. 385–394, 1998.
- [9] D. Debnath and K. Chatterjee, "Two-Stage Solar Photovoltaic-Based Stand-Alone Scheme Having Battery as Energy Storage Element for Rural Deployment," *IEEE Trans. Ind. Electron.*, vol. 62, no. 7, pp. 4148–4157, 2015.
- [10] S. Xue, L. Zhang, W. Xu, S. Member, K. Yu, W. Chen, S. Member, and L. Zhang, "Flexible Power Distribution Control in an," vol. 65, no. 8, pp. 6150–6159, 2018.
- [11] J. Asakura and H. Akagi, "State-of-Charge (SOC)-Balancing Control of a Battery Energy Storage System Based on a Cascade PWM Converter," *IEEE Trans. Power Electron.*, vol. 24, no. 6, pp. 1628–1636, 2009.
- [12] C. Young, N. Chu, and S. Member, "A Single-Phase Multilevel Inverter," vol. 60, no. 5, pp. 1972–1978, 2013.
- [13] H. Zhou, T. Bhattacharya, D. Tran, T. S. T. Siew, and A. M. Khambadkone, "Composite energy storage system involving battery and ultracapacitor with dynamic energy management in microgrid applications," *IEEE Trans. Power Electron.*, vol. 26, no. 3, pp. 923–930, 2011.
- [14] Z. Zheng, K. Wang, L. Xu, and Y. Li, "A hybrid cascaded multilevel converter for battery energy management applied in electric vehicles," *IEEE Trans. Power Electron.*, vol. 29, no. 7, pp. 3537–3546, 2014.
- [15] L. M. Tolbert, S. Member, F. Z. Peng, T. Cunyngnam, and J. N. Chiasson, "Charge Balance Control Schemes for Cascade Multilevel Converter in Hybrid Electric Vehicles," *October*, vol. 49, no. 5, pp. 1058–1064, 2002.
- [16] M. Vasiladiotis and A. Rufer, "Analysis and Control of Modular Multilevel Converters With Integrated Battery Energy Storage," *IEEE Trans. Power Electron.*, vol. 30, no. 1, pp. 163–175, 2015.
- [17] M. C. P. System, G. Farivar, S. Member, B. Hredzak, and S. Member, "A DC-Side Sensorless Cascaded H-Bridge," vol. 63, no. 7, pp. 4233–4241, 2016.
- [18] C. D. Fuentes, C. A. Rojas, H. Renaudineau, S. Kouro, M. A. Perez, and M. Thierry, "Experimental Validation of a Single DC Bus Cascaded H-bridge Multilevel Inverter for Multistring Photovoltaic Systems," *IEEE Trans. Ind. Electron.*, vol. 64, no. 2, pp. 930–934, 2016.
- [19] E. Villanueva, P. Correa, J. Rodríguez, S. Member, M. Pacas, and S. Member, "Control of a Single-Phase Cascaded H-Bridge Multilevel Inverter for Grid-Connected Photovoltaic Systems," vol. 56, no. 11, pp. 4399–4406, 2009.
- [20] J. Ferrieux and Y. Lembeye, "Optimization and Design of a Cascaded DC / DC Converter Devoted to Grid-Connected Photovoltaic Systems," vol. 27, no. 4, pp. 2018–2027, 2018.
- [21] G. I. U. Level-shifted, P. Pwms, J. Chavarria, D. Biel, F. Guinjoan, C. Meza, and J. J. Negroni, "Energy-Balance Control of PV Cascaded Multilevel," vol. 60, no. 1, pp. 98–111, 2013.
- [22] B. Xiao, S. Member, L. Hang, J. Mei, C. Riley, S. Member, L. M. Tolbert, B. Ozpineci, and S. Member, "Modular Cascaded H-Bridge Multilevel PV Inverter With Distributed MPPT for Grid-Connected Applications," vol. 51, no. 2, pp. 1722–1731, 2015.
- [23] J. A. Ferreira, "Nestled Secondary Power Loops in Multilevel Modular Converters," pp. 1–9.
- [24] K. Huang and J. A. Ferreira, "Two Operational Modes of the Modular Multilevel DC Converter," pp. 1347–1354, 2015.
- [25] J. a. Ferreira, "The multilevel modular DC converter," *IEEE Trans. Power Electron.*, vol. 28, no. 10, pp. 4460–4465, 2013.
- [26] W. Jiang, L. Huang, L. Zhang, H. Zhao, L. Wang, and W. CHEN, "Control of Active Power Exchange With Auxiliary Power Loop in Single-Phase Cascaded Multilevel Converter Based Energy Storage System," *IEEE Trans. Power Electron.*, vol. 32, no. 2, pp. 1–1, 2016.